buildings

MDPI

Article

Method for Determining the Fracture Parameters of Fully Graded Dam Concrete

Xiaofeng Gao [1,2,*], Jiong Wu [1], Mengxia Zhou [3,4], Tao Xu [1], Chunfeng Liu [3,4], Yaosheng Tan [3,4], Ning Yang [3,4] and Yu Qiao [3,4]

[1] College of Civil Engineering, Zhejiang University of Technology, Hangzhou 310023, China
[2] State Key Laboratory of Hydroscience and Engineering, Tsinghua University, Beijing 100084, China
[3] China Three Gorges Construction Engineering Corporation, Chengdu 610041, China
[4] China Three Gorges Group Corporation, Beijing 100038, China
* Correspondence: gaoxf@zjut.edu.cn; Tel.: +86-571-85290813

Abstract: This paper describes a method for determining the initiation and unstable toughness of fully graded concrete of arbitrary specimen size. The method first predicts the initiation and peak loads of concrete specimens of any size, as well as crack length-to-height ratios based on the fracture test results of concrete specimens with limited sizes or crack length-to-height ratios. Then, combined with the fracture extreme theory, the fracture toughness of concrete with varying size or crack length-to-height ratios is determined. Finally, in order to verify the applicability of the method, it is used to calculate the fracture toughness of small aggregate concrete and fully graded concrete with different sizes or crack length-to-height ratios, and its prediction accuracy is evaluated through indices such as mean absolute percentage error, root mean square error and reliability index a15. The results show that the proposed method can meet the needs of practical engineering applications and can provide theoretical basis for the optimization of the fracture test method of fully graded concrete and the determination of fracture parameters in crack stability or propagation analysis.

Keywords: hydraulic structure; fully graded; fracture parameters; size effect; fracture extreme theory

Citation: Gao, X.; Wu, J.; Zhou, M.; Xu, T.; Liu, C.; Tan, Y.; Yang, N.; Qiao, Y. Method for Determining the Fracture Parameters of Fully Graded Dam Concrete. *Buildings* **2023**, *13*, 24. https://doi.org/10.3390/buildings13010024

Academic Editor: Tomáš Dvorský

Received: 15 November 2022
Revised: 13 December 2022
Accepted: 19 December 2022
Published: 22 December 2022

1. Introduction

In order to ensure the safe operation of dam structures, it is necessary to study the mechanical parameters of dam concrete under actual service conditions. Existing studies have shown that factors such as environment [1–3], concrete raw materials [4,5], and curing conditions [6] affect the toughness, strength, and elastic modulus of dam concrete. Among all of the above mechanical properties, fracture toughness is an important index to evaluate the crack resistance of dam concrete [7]. Generally, it can be determined by the wedge-splitting method [5,8,9] or the three-point bending-beam method [10–12]. Based on the double-*K* fracture theory proposed by Xu et al. [13–15], the National Development and Reform Commission of China [16] and RILEM [17] developed a concrete fracture test standard. The double-*K* fracture theory uses the initiation and unstable toughness to describe the whole process of concrete structure crack from initiation and crack propagation to unstable failure. Existing research shows that the double-*K* fracture toughness of concrete measured by this test may have a size effect [18–21], and the larger the maximum particle size of concrete aggregate, the larger the minimum specimen size required to determine the stable fracture toughness. For fully graded concrete with a maximum aggregate size of 150 mm, when the stable fracture toughness is determined by the wedge-splitting method, the required minimum specimen height should be 1.5 m [7,21,22]. The fracture testing of large-size specimens is associated with problems such as high equipment requirements, difficult testing, and inaccurate testing [22,23], so it is difficult to carry out normal tests at engineering sites. If a method can be found to determine the double-*K* fracture toughness of any size of specimen based on the fracture test results of smaller concrete specimens, it can

provide a basis for the optimization of the fracture test of fully graded concrete. According to the double-*K* fracture toughness calculation formula, the initiation toughness is related to the initiation load and the initial crack length, whereas the calculation of the unstable toughness requires the peak load and the effective crack length. Therefore, the key is to solve the problem of how to determine the initiation load, peak load and effective crack length of specimens of any size through the fracture test results of smaller specimens.

In order to predict the fracture failure of quasi-brittle material specimens, scholars have proposed different theoretical models. The most famous ones are the boundary effect model proposed by Hu et al. [24–26] and the size effect model proposed by Bažant et al. [27–29]. Based on the boundary effect model, Guan et al. [30] established a linear formula between the peak load of concrete with different sizes or α_c and tensile strength, where α_c is the crack length-to-height ratio. Furthermore, Yao and Guan et al. [31–33] proposed the concept of cracking strength and established a linear expression between the initiation load and the cracking strength of concrete specimens when the size or α_c changes. Guan et al. [10,34] also established the relationship between fracture toughness and the failure curve based on the improved boundary effect model. The above initiation and peak load prediction methods based on the boundary effect model are currently used for small aggregate concrete. For fully graded concrete, Gao et al. [7] established a linear relationship between the nominal initiation strength, nominal unstable strength and the height of the specimen based on the type 2 size effect model. By introducing the equivalent geometric parameters, the prediction formula of initiation and peak loads of concrete specimens is proposed when the size or α_c changes, so as to realize the prediction of initiation and peak loads of specimens with any size or α_c. Although the basic assumptions of the boundary effect and the size effect model are different, the predicted results obtained by the two are basically consistent. In this study, the size effect model is selected as the method to determine the initiation and peak loads of concrete specimens when the size or α_c changes.

After determining the initiation and peak loads of any size of specimen, the initiation toughness can be directly obtained by the initiation load and the initial crack length, whereas the calculation of the unstable toughness requires the critical crack length (a_c). Because the predicted fracture results based on the size effect model cannot yield a_c, it needs to be obtained by establishing and solving the equations of the critical state of concrete specimens. Based on a fictitious crack model, Wu et al. [35,36] established the equilibrium equation of force and moment in the midspan section of a three-point bending beam and obtained a_c with the flexural tensile strength of concrete as the known quantity. In order to determine the fracture parameters of concrete more easily and reliably, Qing et al. proposed a fracture extreme theory that can determine a_c and other fracture parameters only based on the peak load of fracture test [37–47]. The theory assumes that the partial derivative of the F_H to crack length is continuous when F_H reaches the peak load during the fracture process of concrete, and the derivative of F_H to crack length is zero at the extreme point. Furthermore, based on the relationship between F_H and a under the peak load state, combined with several other equations, the a_c and other fracture parameters of specimens of different sizes can be determined. The accuracy of fracture extreme value theory for predicting fracture parameters of concrete has been widely verified. Accordingly, a_c can be easily and reliably determined by fracture extreme value theory with only the peak load. Therefore, after the peak load is determined, the fracture extreme theory proposed by Qing et al. is an effective method to solve for the critical crack length a_c of any size specimen.

In summary, based on the fracture test results of concrete specimens with limited size and α_c, the size effect model can be used to predict the initiation and peak loads of concrete specimens with any size or α_c, and combined with the fracture extreme theory, the initiation and unstable toughness of concrete specimens can be calculated when the size or α_c changes. Although this method is theoretically feasible, its applicability and accuracy still need to be verified by test results. In this paper, we first introduce the determination method of fracture parameters and then verify the applicability and accuracy of the method using the fracture test results of small aggregate concrete and fully graded large aggregate

concrete. The research results presented in this paper can provide a theoretical basis for the optimization of the fracture test at the engineering site, as well as for the determination of fracture parameters in crack stability or propagation analysis.

2. Determination Method of Fracture Parameters

The fracture parameter determination method proposed in this paper is based on the test results of concrete specimens with limited size or α_c. The size effect model is used to predict the initiation and peak loads of concrete specimens with an arbitrary size or α_c. Then, the predicted value of the peak load is taken as the known condition, and the critical crack length is determined according to the fracture extreme theory. Finally, the initiation and unstable toughness of concrete specimens are determined based on the predicted initiation load and initial crack length and the predicted peak load and critical crack length, respectively, when the specimen size or α_c changes. The calculation flow chart is shown in Figure 1. This method can be used to analyze the fracture test results of different specimens, such as those obtained by the wedge-splitting method, the three-point bending-beam method and the compact tension method. Considering that the self-weight of fully graded concrete specimens is generally large, the wedge-splitting method is used to determine the fracture parameters, which can overcome the influence of the self-weight of the specimen on the fracture process. Therefore, the applicability and accuracy of the method are verified by the wedge-splitting fracture test results in the literature. The formula for calculating the initiation and unstable toughness of wedge-splitting specimens given by the "Norm for fracture test of hydraulic concrete" [16] in China is as follows:

$$K_{IC}^{Q} = \frac{F_{HQ} \times 10^{-3}}{th^{1/2}} f(\alpha_0) = Y(\alpha_0)\sigma_N^{Q}\sqrt{\pi a_0} \tag{1}$$

$$\sigma_N^{Q} = \frac{4F_{HQ} \times 10^{-3}}{th} \tag{2}$$

$$K_{IC}^{S} = \frac{F_{Hmax} \times 10^{-3}}{th^{1/2}} f(\alpha_c) = Y(\alpha_c)\sigma_N^{S}\sqrt{\pi a_c} \tag{3}$$

$$\sigma_N^{S} = \frac{4F_{Hmax} \times 10^{-3}}{th} \tag{4}$$

$$Y(\alpha) = \frac{f(\alpha)}{4\sqrt{\pi\alpha}} = \frac{3.675[1 - 0.12(\alpha - 0.45)]}{4\sqrt{\pi\alpha}(1-\alpha)^{3/2}} \tag{5}$$

where K_{IC}^{Q} and K_{IC}^{S} are the initiation toughness and unstable toughness, respectively (MPa·m$^{1/2}$); F_{HQ} and F_{Hmax} are the initiation load and peak load, respectively (kN); $f(\alpha_0)$ and $Y(\alpha_0)$ are the dimensionless geometric parameters of the specimen; a_c is the critical crack length when the specimen reaches the peak load (m); α_c is the crack length-to-height ratio ($\alpha_c = a_c/h$); and σ_N^{Q} and σ_N^{S} are the nominal initiation and unstable strength, respectively, i.e., the maximum tensile stress of the fracture surface caused by the initiation load and peak load without considering the existence of an initial crack (MPa).

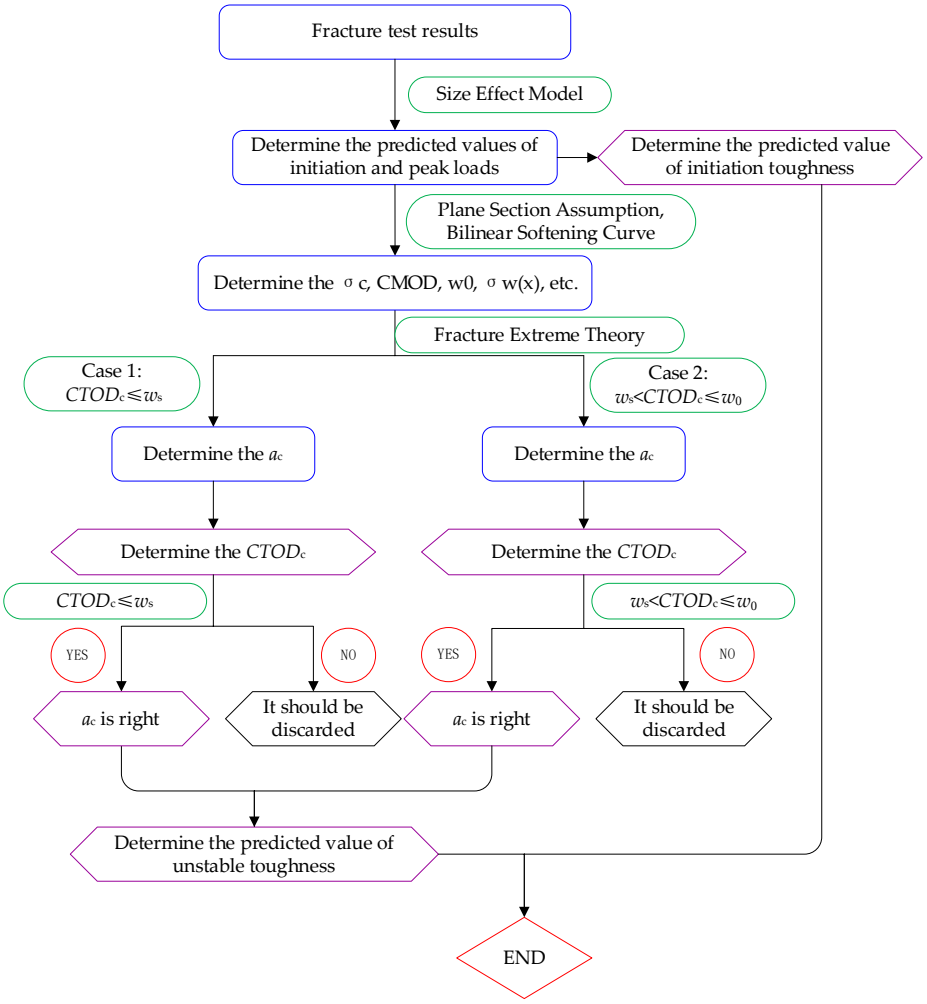

Figure 1. Calculation flow chart.

2.1. Determination of Initiation Load and Peak Load

In this paper, the size effect model is selected as the method to determine the initiation and peak loads of concrete specimens when the size or α_c changes. The evolution form of the type 2 size effect model proposed by Gao et al. [48] can be used to analyze the size effect of fracture test results in geometrically similar specimens. On this basis, in order to analyze the test results when the specimen size or α_c changes, the linear equations of nominal strength and equivalent crack length as shown in Equations (6) and (7) can be established [48].

$$\frac{1}{\left(\sigma_{\mathrm{Ne}}^{\mathrm{Q}}\right)^2} = \frac{1}{\left(K_{\mathrm{IC}}^{\mathrm{ini}}\right)^2} a_{\mathrm{e}} + \frac{c_{\mathrm{f}}^{\mathrm{ini}}}{\left(K_{\mathrm{IC}}^{\mathrm{ini}}\right)^2} = A_1 a_{\mathrm{e}} + C_1 \tag{6}$$

$$\frac{1}{\left(\sigma_{\mathrm{Ne}}^{\mathrm{S}}\right)^2} = \frac{1}{\left(K_{\mathrm{IC}}^{\mathrm{un}}\right)^2} a_{\mathrm{e}} + \frac{c_{\mathrm{f}}^{\mathrm{un}}}{\left(K_{\mathrm{IC}}^{\mathrm{un}}\right)^2} = A_2 a_{\mathrm{e}} + C_2 \tag{7}$$

where $\sigma_{\mathrm{Ne}}^{\mathrm{Q}}$ and $\sigma_{\mathrm{Ne}}^{\mathrm{S}}$ are equivalent nominal initiation strength and equivalent nominal unstable strength, respectively ($\sigma_{\mathrm{Ne}}^{\mathrm{Q}} = \sigma_{\mathrm{N}}^{\mathrm{Q}} H(\alpha)\pi^{1/2}$, $\sigma_{\mathrm{Ne}}^{\mathrm{S}} = \sigma_{\mathrm{N}}^{\mathrm{S}} H(\alpha)\pi^{1/2}$) (MPa); a_{e} is the equivalent crack length ($a_{\mathrm{e}} = Y^2(\alpha_0)/H^2(\alpha_0) \times a_0$, m, $H(\alpha_0) = \left[Y^2(\alpha_0) + 2Y(\alpha_0) \times Y'(\alpha_0) \times \alpha_0\right]^{1/2}$); and A_1, A_2, C_1 and C_2 are the parameters of two linear equations, which can be determined by fitting the test results.

Based on the experimental F_{HQ} and F_{Hmax}, the linear relationship between $1/\left(\sigma_{\mathrm{Ne}}^{\mathrm{Q}}\right)^2$, $1/\left(\sigma_{\mathrm{Ne}}^{\mathrm{S}}\right)^2$ and a_{e} can be established by Equation (6) and Equation (7), respectively. Ac-

cording to the slope and intercept of the two linear equations, the initiation toughness without the size effect (K_{IC}^{ini}), the effective length of the initiation fracture process zone (c_f^{ini}), the unstable toughness without the size effect (K_{IC}^{un}), and the effective length of the unstable fracture process zone (c_f^{un}) can be calculated; $K_{IC}^{ini} = 1/(A_1)^{1/2}$, $c_f^{ini} = C_1/A_1$, $K_{IC}^{un} = 1/(A_2)^{1/2}$, $c_f^{un} = C_2/A_2$.

Furthermore, Gao et al. [7] introduced the equivalent geometric parameters into the size effect model and established the prediction formulas of initiation and peak loads when the size or α_c of a concrete specimen changed, as shown in Equations (8) and (9).

$$F_{HQ}^{Pre} = \frac{ht \times 10^3}{4\sqrt{g'(\alpha_0)c_f^{ini} + g(\alpha_0)h}} K_{IC}^{ini} = A_e^{ini} K_{IC}^{ini} \tag{8}$$

$$F_{Hmax}^{Pre} = \frac{ht \times 10^3}{4\sqrt{g'(\alpha_0)c_f^{un} + g(\alpha_0)h}} K_{IC}^{un} = A_e^{un} K_{IC}^{un} \tag{9}$$

where F_{HQ}^{Pre} and F_{Hmax}^{Pre} are the initiation and peak load prediction, respectively; $g(\alpha_0)$ and $g'(\alpha_0)$ are the dimensionless geometric parameters of the specimen ($g(\alpha_0) = Y^2(\alpha_0)\pi\alpha_0$, $g'(\alpha_0) = H^2(\alpha_0)\pi$); and A_e^{ini} and A_e^{un} are equivalent geometric parameters related to initiation and instability, respectively (mm·m$^{1/2}$). Other parameters are the same as the previous definition.

2.2. Determination of Initiation Toughness and Unstable Toughness

After the F_{HQ}^{Pre} and F_{Hmax}^{Pre} are determined, the K_{IC}^{Q} can be calculated directly according to Equation (1). For K_{IC}^{S}, a_c should be calculated first according to fracture extreme theory and substituted into Equation (3) to determine K_{IC}^{S}. According to the fracture extreme theory, at the extreme point, the derivative of F_H to a is zero [37], namely:

$$\left.\frac{\partial F_H}{\partial a}\right|_{a=a_c} = 0 \tag{10}$$

The functional relationship between F_H and a can be established by fracture propagation criterion equation in the critical state of concrete or the equilibrium equation of a ligament section. By combining the established function relation and Equation (10), a_c can be solved. In this paper, the functional relationship between F_H and a is established by using the equilibrium equation of force and moment of ligament section. Based on a fictitious crack model, Wu [35] and Qing [39] obtained the stress and strain distributions of ligament sections of three-point bending-beam specimens and wedge-splitting specimens, as shown in Figure 2.

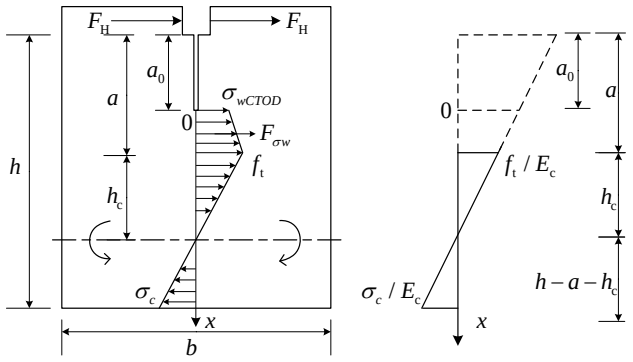

Figure 2. Stress and strain distribution in a ligament cross section of a wedge-splitting specimen.

According to the stress distribution shown in Figure 2, with the initial crack tip as the coordinate origin, the force and moment equilibrium equation of the ligament section shown in Equations (11) and (12), respectively, can be obtained [35,39]:

$$\frac{1}{2}\sigma_c t(h-a-h_c)+F_H\times 10^{-3}=\frac{1}{2}f_t t h_c+\int_0^{a-a_0}\sigma_w t dx \tag{11}$$

$$\frac{1}{3}\sigma_c t(h-a-h_c)^2+\frac{1}{3}f_t t h_c^2+\int_0^{a-a_0}\sigma_w t(h_c+a-a_0-x)dx=F_H(a+h_c)\times 10^{-3} \tag{12}$$

where σ_c is the compressive stress at the bottom of the specimen (MPa); t is the thickness of specimen (m); h is the effective height of the specimen (m); a_0 and a are initial crack length and effective crack length, respectively (m); h_c is the distance from the crack tip to the neutral axis marked by the dotted line in Figure 2 (m); f_t is the equivalent tensile stress at the crack tip, namely the equivalent tensile strength (MPa); and σ_w is the cohesive force in the fracture process zone (MPa).

According to the plane section assumption and the strain distribution shown in Figure 2, the expression of σ_c is obtained as follows [35,39]:

$$\sigma_c=\frac{f_t(h-a-h_c)}{h_c} \tag{13}$$

According to the assumption that the crack-opening surface remains a plane [35,39], the relationship between the virtual crack-opening displacement ($w(x)$) and the crack-tip opening displacement ($CTOD$, $w(x)$), as well as the crack-mouth-opening displacement ($CMOD$) can be established as:

$$w(x)=\left(1-\frac{x}{a-a_0}\right)CTOD \tag{14}$$

$$CTOD=\frac{a-a_0}{a}CMOD \tag{15}$$

where $CMOD$ can be obtained according to the empirical calculation proposed by Xu et al. [15].

$$CMOD=\frac{F_H}{tE_c}\left[13.18\left(1-\frac{a}{h}\right)^{-2}-9.16\right] \tag{16}$$

The relationship between the cohesive force in the fracture process zone and the virtual fracture-opening displacement can be characterized by the tensile softening curve [49], which often adopts a bilinear, exponential, power function, curve or other form. The bilinear softening curve shown in Figure 3 is used in this paper.

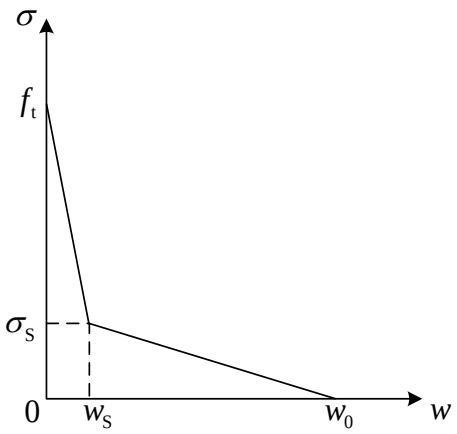

Figure 3. Bilinear softening curve.

The function expression of the bilinear softening curve is expressed as follows:

$$\sigma_w(x) = \begin{cases} f_t - (f_t - \sigma_s)w(x)/w_s & 0 \le w(x) \le w_s \\ \sigma_s(w_0 - w(x))/(w_0 - w_s) & w_s \le w(x) \le w_0 \end{cases} \tag{17}$$

where $w(x)$, w_s and w_0 are the crack-opening displacement at x, the crack-opening displacement at the inflection point of the bilinear softening relationship and the crack-opening displacement at zero cohesion, respectively (μm); and $\sigma_w(x)$ and σ_s are the cohesive force at x and the inflection point, respectively (MPa). The values of σ_s, w_s and w_0 in the formula can be calculated using the assumption proposed by Wittmann et al. [50]:

$$\begin{cases} \sigma_s = f_t/4 \\ w_s = 0.75G_f/f_t \\ w_0 = 5G_f/f \end{cases} \tag{18}$$

In order to reduce the parameters used in the calculation process, in combination with Equation (18), Equation (17) can be rewritten as follows:

$$\sigma_w(x) = \begin{cases} f_t(1 - 5w(x)/w_0) & 0 \le w(x) \le w_s \\ \frac{5}{17}f_t(1 - w(x)/w_0) & w_s \le w(x) \le w_0 \end{cases} \tag{19}$$

In the tensile softening curve, the crack-opening displacement (w_0), which characterizes the zero cohesion, is the material constant, and its value can be generally determined by the direct tensile test [51] or empirical formula [52]. For concrete materials, the variation range of w_0 provided by multiple scholars is large [51–53], mostly between 100 and 1000 μm. Owing to the difficulty of conducting a direct tensile test on fully graded concrete [54] and because the specific empirical formula may not be applicable to different types of concrete materials, in this paper, we determine w_0 using the best fitting method. First, w_0 is selected from 100 to 1000 μm at 50 μm intervals; then, a_c and K_{IC}^S can be calculated according to the fracture extreme theory. When the overall error between the calculated K_{IC}^S and the test results is the smallest, the corresponding w_0 is the best crack-opening displacement at zero cohesion of concrete.

Equation (14) is substituted into (19) to obtain the expression of the cohesion distribution function in the fracture process area, and a_c can be calculated. The $\sigma_w(x)$ selected in this paper is the bilinear softening curve. Therefore, the relationship between $w(x)$ and w_s at the inflection point of the bilinear softening relationship needs to be discussed when determining the stress distribution in the fracture process area. Obviously, under the peak load state, the maximum value of $w(x)$ is $CTOD$, which is located at the initial crack tip, whereas the minimum value of $w(x)$ is 0, which is located at the equivalent crack tip. When $CTOD_c \le w_s$, the cohesion from the initial crack tip to the equivalent crack tip is a linear distribution, whereas when $w_s < CTOD_c \le w_0$, the cohesion is a bilinear distribution. The following two situations are discussed.

Case 1: $CTOD_c \le w_s$. Figure 4 shows the cohesive stress distribution and the corresponding softening relationship in the fracture process zone when $CTOD_c \le w_s$.

Substituting Equation (14) into (19), the cohesive stress distribution function in the fracture process zone of Case 1 can be obtained as:

$$\sigma_w(x) = f_t\left[1 - 5\left(1 - \tfrac{x}{a-a_0}\right)\tfrac{CTOD}{w_0}\right] \quad (0 \le x \le a - a_0) \tag{20}$$

Substituting Equations (13) and (20) into (11), the distance from the equivalent crack tip to the neutral axis (h_c) can be obtained as:

$$h_c = \frac{(h-a)^2}{2\left[(a-a_0)\left(1 - \frac{5CTOD}{2w_0}\right) + h - a - \frac{F_H \times 10^{-3}}{f_t t}\right]} \tag{21}$$

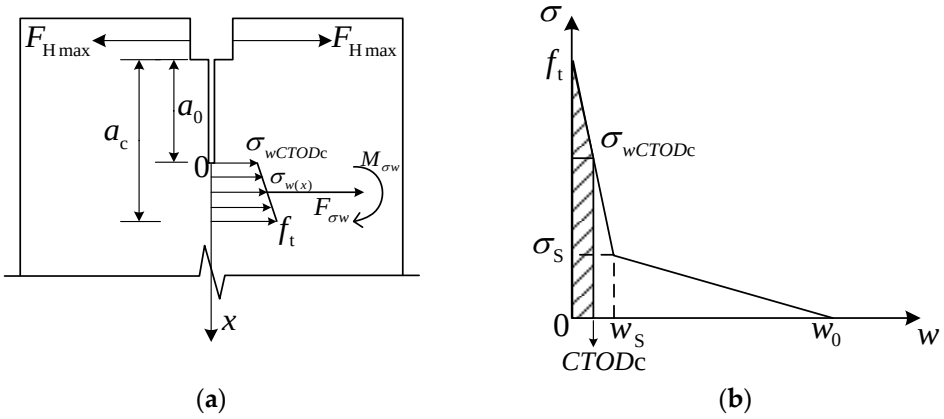

Figure 4. Case 1: (**a**) cohesive stress distribution; (**b**) softening curve.

The functional relationship between F_H and a can be obtained by substituting Equations (13) and (20) into (12):

$$\frac{F_H(a+h_c)\times 10^{-3}}{f_t t} = (a-a_0)\left[(a-a_0)\left(\frac{1}{2}-\frac{5CTOD}{3w_0}\right)+h_c\left(1-\frac{5CTOD}{2w_0}\right)\right]+ \frac{(h-a)^3}{3h_c}-(h-a)^2+(h-a)h_c \tag{22}$$

Furthermore, by substituting Equations (15), (16) and (21) into (22), a function containing only F_H, a and f_t is obtained. According to the fracture extreme theory, the partial derivative of F_H to a is zero at the extreme point. Substituting $a = a_c$ and $F_H = F_{Hmax}$ into Equations (10) and (22), a_c can be obtained; then, $CTOD_c$, K_{IC}^S and other parameters can be calculated. If the calculated $CTOD_c \le w_s$, a_c is the real solution, and on the contrary, it should be discarded.

Case 2, $w_s < CTOD_c \le w_0$. Figure 5 shows the cohesive force distribution and the corresponding softening relationship in the fracture process zone when $w_s < CTOD_c \le w_0$.

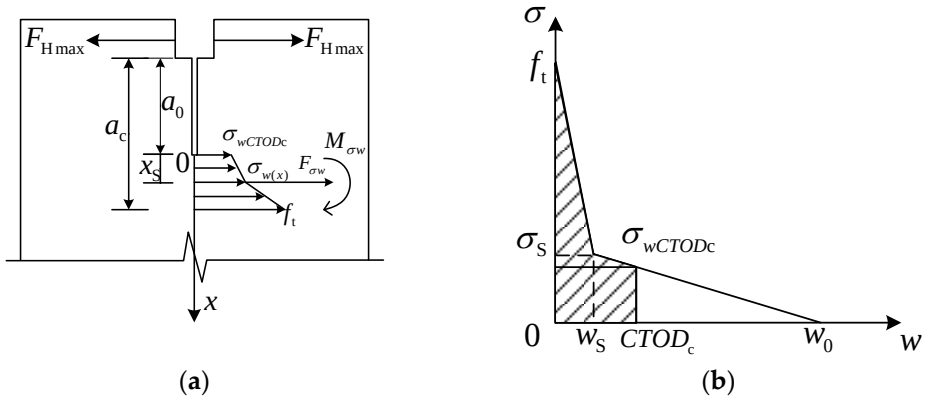

Figure 5. Case 2: (**a**) cohesive stress distribution; (**b**) softening curve.

Figure 5a shows that the cohesive force is a bilinear distribution, and the coordinate (x_s) of the turning point can be calculated according to the following formula:

$$x_s = (a-a_0)\left(1-\frac{3w_0}{20CTOD}\right) \tag{23}$$

Similar to Case 1, the cohesive force distribution function in the fracture process zone of Case 2 can be obtained by substituting Equation (14) into (19):

$$\sigma_w(x) = \begin{cases} \frac{5}{17} f_t \left[1 - \left(1 - \frac{x}{a-a_0}\right)\frac{CTOD}{w_0}\right] & 0 \le x \le x_s \\ f_t \left[1 - 5\left(1 - \frac{x}{a-a_0}\right)\frac{CTOD}{w_0}\right] & x_s \le x \le a - a_0 \end{cases} \tag{24}$$

Furthermore, the distance from the crack tip to the neutral axis is:

$$h_{c2} = \frac{(h-a)^2}{2[-\frac{12}{17}x_s + \frac{80CTODx_s}{17w_0} - \frac{40CTODx_s^2}{17w_0(a-a_0)} - \frac{5(a-a_0)CTOD}{2w_0} + h - a_0 - \frac{F_H \times 10^{-3}}{f_t t}]} \tag{25}$$

By substituting Equations (13) and (24) into (12), the relation between the Case 2 F_H and a is obtained:

$$\begin{aligned} &\frac{F_H(a+h_c)\times 10^{-3}}{f_t t} = \frac{(h-a)^3}{3h_c} - (h-a)^2 + (h-a)h_c + \frac{5}{17}x_s\left(1 - \frac{CTOD}{w_0}\right)(h_c + a - a_0) - \\ &\frac{5}{34}x_s^2\left[1 - \frac{2CTOD}{w_0} - \frac{h_c CTOD}{(a-a_0)w_0}\right] - \frac{5x_s^3 CTOD}{51(a-a_0)w_0} + (a - a_0 - x_s)(h_c + a - a_0)\left(1 - \frac{5CTOD}{w_0}\right) - \\ &\frac{5\left[(a-a_0)^3 - x_s^3\right]CTOD}{3(a-a_0)w_0} - \frac{1}{2}\left[(a-a_0)^2 - x_s^2\right]\left[1 - \frac{10CTOD}{w_0} - \frac{5h_c CTOD}{(a-a_0)w_0}\right] \end{aligned} \tag{26}$$

By substituting Equations (15), (16), (23) and (25) into (26), a functional equation containing only F_H, a and f_t can be obtained. By substituting $a = a_c$ and $F_H = F_{Hmax}$ into Equations (10) and (26), respectively, parameters such as a_c and K_{IC}^S can be obtained. If the calculated $CTOD_c$ satisfies condition 2, a_c is the real solution, and on the contrary, it should be discarded.

According to the above calculation process, a_c and K_{IC} corresponding to a specific w_0 can be obtained. By repeating the above process, the best w_0 value with the smallest overall error between K_{IC}^S and test results can be determined. The error or prediction accuracy can be evaluated using the indicators commonly used in engineering.

2.3. Evaluation Index of Model Prediction Accuracy

The root mean square error (*RMSE*), mean absolute percentage error (*MAPE*) and reliability index a_{15} were used to evaluate the prediction accuracy of the model. The calculation formula of each indicator is as follows:

$$RMSE = \sqrt{\frac{1}{n}\sum_{i=1}^{n}(\hat{y}_i - y_i)^2} \tag{27}$$

$$MAPE = \frac{1}{n}\sum_{i=1}^{n}\left|\frac{\hat{y}_i - y_i}{y_i}\right| \times 100\% \tag{28}$$

$$a15 = \frac{m15}{M} \tag{29}$$

$$Cov(y_i, \hat{y}_i) = E[y_i\hat{y}_i] - E[y_i]E[\hat{y}_i] \tag{30}$$

where n is the amount of data points; i is the number of the data point; y_i and $\hat{y}_i$ are the measured and predicted values of the i-th data point, respectively; a_{15} is the proportion of samples with deviation within ±15% compared with the test results; $m15$ and M are the number of samples with prediction error less than ±15% and the number of samples in the dataset, respectively; $Cov(y_i, \hat{y}_i)$ is the covariance of the measured and predicted values; and $E[y_i]$ and $E[\hat{y}_i]$ are the expected values of the measured and predicted values, respectively.

3. Method Validation and Discussion

In this section, four groups of fracture test results of different sizes and the α_c of small aggregate concrete and Wudongde fully graded concrete are selected to verify the applicability and accuracy of the proposed method.

3.1. Small Aggregate Concrete

3.1.1. Same Crack Length-to-Height Ratio and Different Specimen Sizes

(1) α_0 = 0.4, h = 0.2~1 m

In order to study the influence of specimen size on the fracture performance of concrete, a fracture test was carried out in [55] on wedge-splitting tensile specimens with a maximum aggregate particle size of 25 mm, an effective specimen height ranging from 0.2 m to 1 m and an initial α_c of 0.4. Table 1 shows the specimen size information and test results. The elastic modulus of concrete (E_c = 30.7 GPa) was obtained by the conversion of cube compressive strength. Additional experimental information can be found in reference [55].

Table 1. Fracture test results reported in reference [55].

Specimen Number	h/m	b/m	α_0	F_{HQ}/kN	F_{Hmax}/kN
200-1	0.20	0.20	0.40	7.85	10.02
200-2	0.20	0.20	0.40	7.81	10.69
200-3	0.20	0.20	0.40	7.65	9.62
200-4	0.20	0.20	0.40	9.27	10.60
200-6	0.20	0.20	0.40	8.65	10.93
300-1	0.30	0.20	0.40	9.97	15.33
300-2	0.30	0.20	0.40	10.45	14.78
300-3	0.30	0.20	0.48	10.00	12.56
300-4	0.30	0.20	0.40	11.31	15.12
300-5	0.30	0.20	0.40	8.90	12.06
600-1	0.60	0.21	0.40	20.47	26.68
600-2	0.61	0.22	0.44	19.20	28.13
600-3	0.60	0.22	0.40	15.84	27.02
600-4	0.60	0.22	0.40	22.90	29.12
600-5	0.60	0.21	0.48	28.17	28.66
600-6	0.61	0.21	0.44	26.49	31.50
800-1	0.81	0.24	0.43	31.47	34.69
800-2	0.81	0.25	0.40	30.64	34.99
800-3	0.80	0.24	0.40	20.65	33.72
800-4	0.80	0.24	0.40	22.56	33.96
800-5	0.80	0.23	0.45	33.90	37.83
800-6	0.80	0.23	0.40	23.72	34.25
1000-1	1.01	0.24	0.40	28.75	43.58
1000-2	1.01	0.24	0.40	28.53	46.63
1000-3	1.01	0.27	0.39	38.51	55.91
1000-4	1.01	0.24	0.40	35.15	48.16
1000-5	1.00	0.25	0.40	30.19	45.52
1000-6	1.01	0.27	0.40	37.32	50.47

The linear equations of $1/\left(\sigma_{Ne}^{Q}\right)^2$, $1/\left(\sigma_{Ne}^{S}\right)^2$ and a_e, as shown in Figure 6, can be obtained by linear analysis of the test results using Equations (6) and (7). According to the slope and intercept, the initiation toughness without a size effect (K_{IC}^{ini}) is 1.14 MPa·m$^{1/2}$, the effective length of the initiation fracture process zone (c_f^{ini}) is 56.2 mm, the unstable toughness (K_{IC}^{un}) is 1.81 MPa·m$^{1/2}$ and the effective length of unstable fracture process zone (c_f^{un}) is 108.6 mm.

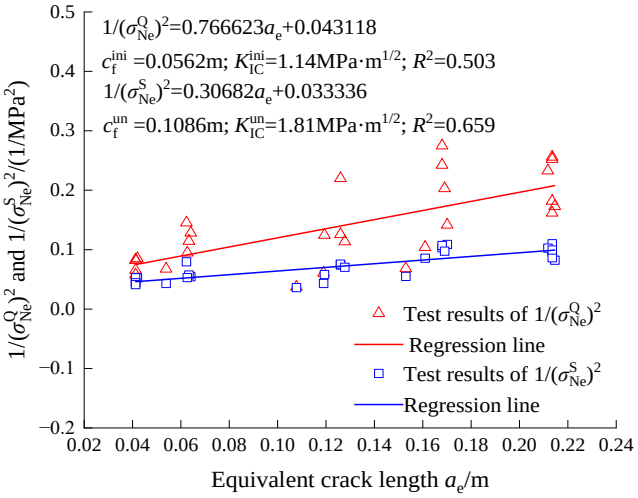

Figure 6. Linear relationships of $1/\left(\sigma_{\mathrm{Ne}}^{\mathrm{Q}}\right)^2$, $1/\left(\sigma_{\mathrm{Ne}}^{\mathrm{S}}\right)^2$ and a_{e}.

The $K_{\mathrm{IC}}^{\mathrm{ini}}$ and $c_{\mathrm{f}}^{\mathrm{ini}}$ and $K_{\mathrm{IC}}^{\mathrm{un}}$ and $c_{\mathrm{f}}^{\mathrm{un}}$ obtained by linear analysis are substituted into Equations (8) and (9), respectively, to obtain the relationship between the initiation and peak loads with the equivalent geometric parameter (A_{e}), as shown in Figure 7. In the figure, the slope of the initiation load prediction line is $K_{\mathrm{IC}}^{\mathrm{ini}}$ without a size effect, and the slope of the peak load prediction line is $K_{\mathrm{IC}}^{\mathrm{un}}$ without a size effect. Figure 7 shows that the test results of F_{HQ} and F_{Hmax} are nearly linear relative to A_{e}. The *MAPE* of the F_{HQ} prediction is 14.29%, the *RMSE* is 4.54 kN, reliability index $a15$ is 67.86% and the covariance is 83.39 (kN)^2. The *MAPE* of the F_{Hmax} prediction is 7.4%, the *RMSE* is 3.05 kN, $a15$ is 85.71% and the covariance is 187.14 (kN)^2. The above indices show that the size effect model can realize the accurate prediction of initiation load and peak load when the size or α_{c} changes.

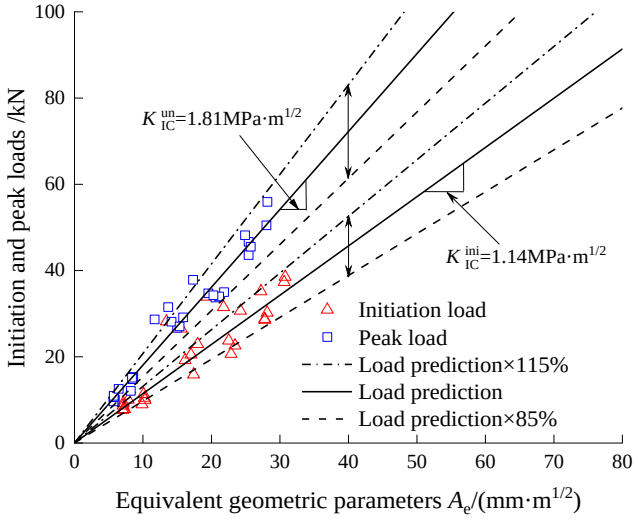

Figure 7. Predicted results of initiation and peak loads.

As mentioned above, in this paper, we use the best fitting method to determine the crack-opening displacement (w_0). In this test, *MAPE* was used to evaluate the prediction accuracy of $K_{\mathrm{IC}}^{\mathrm{S}}$; the calculation results are shown in Figure 8. It can be seen that the minimum *MAPE* is 4.56%, and the corresponding optimal w_0 is 550 μm.

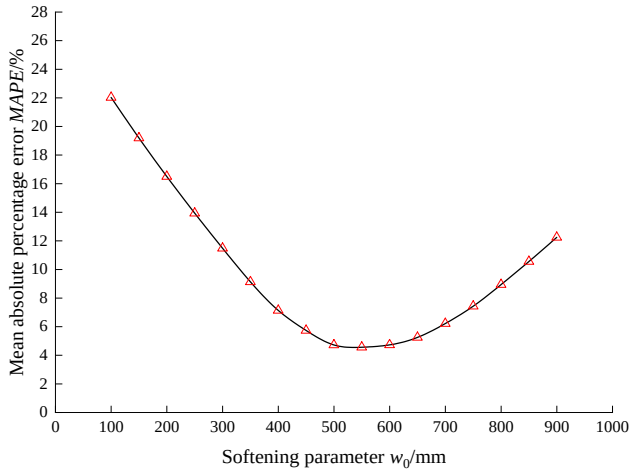

Figure 8. Determination of the softening parameter (w_0).

Based on the optimal w_0 and $F_{\mathrm{Hmax}}^{\mathrm{Pre}}$ obtained above, the critical crack length of specimens of different sizes with an initial α_c of 0.4 was calculated using Equations (3) and (10). Figure 9 shows that each data point is located near the calculated value, with the following corresponding prediction accuracy evaluation indices: $MAPE = 3.42\%$, $RMSE = 0.02$ m, $a15 = 100\%$ and $Cov = 0.02$ m^2.

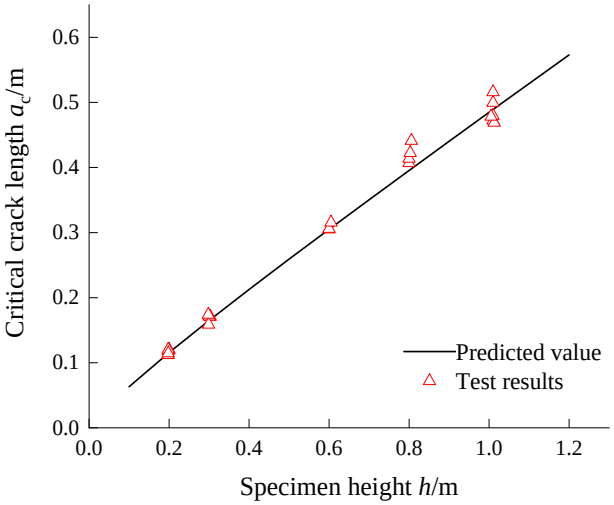

Figure 9. Critical crack length of specimens of different sizes.

Figure 10a shows a comparison between the predicted and test results of unstable toughness ($K_{\mathrm{IC}}^{\mathrm{S}}$), nominal toughness ($K_{\mathrm{IC}}^{\mathrm{N}}$) and initiation toughness ($K_{\mathrm{IC}}^{\mathrm{Q}}$) for specimens of different sizes with an initial α_c of 0.4. The nominal toughness is calculated by substituting the predicted peak load ($F_{\mathrm{Hmax}}^{\mathrm{Pre}}$) and the initial crack length (a_0) into Equation (3). It can be seen from Figure 10a that $K_{\mathrm{IC}}^{\mathrm{S}}$, $K_{\mathrm{IC}}^{\mathrm{N}}$ and $K_{\mathrm{IC}}^{\mathrm{Q}}$ basically increase with the increase in specimen size and gradually stabilize. Among them, $K_{\mathrm{IC}}^{\mathrm{Q}}$ tends toward the initiation toughness without a size effect defined in the size effect model. $K_{\mathrm{IC}}^{\mathrm{S}}$ and $K_{\mathrm{IC}}^{\mathrm{N}}$ tend toward unstable toughness without a size effect, and the difference between them decreases with increased specimen size.

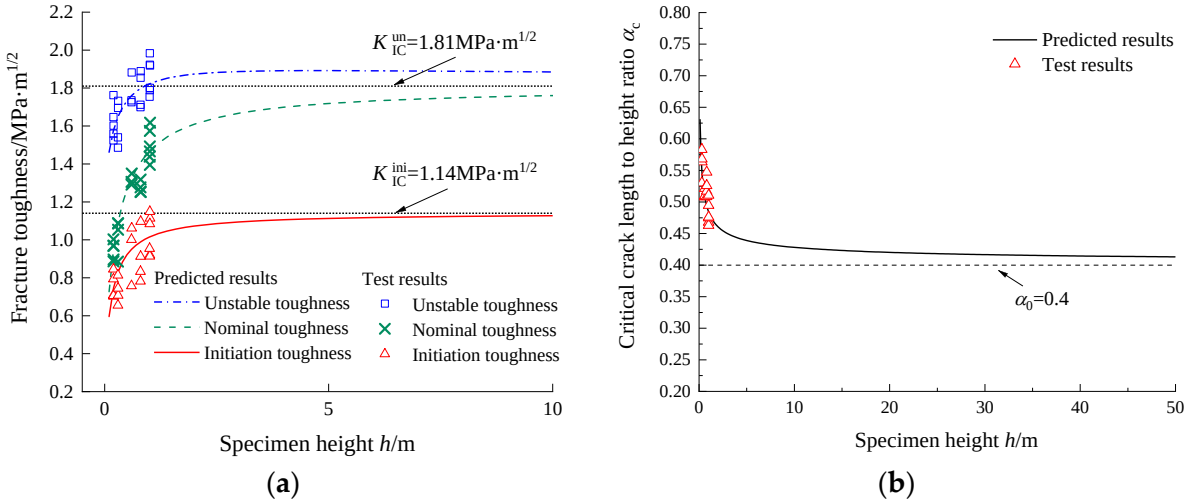

Figure 10. Fracture toughness and crack length-to-height ratio of specimens with different sizes: (**a**) fracture toughness; (**b**) critical crack length-to-height ratios.

This is mainly because the difference between K_{IC}^{S} and K_{IC}^{N} lies in the selection of crack length in toughness calculation. It can be seen from Figure 10b that with the increase in specimen size, α_c gradually approaches α_0. A comparison of the predicted results with the test results shows that the predicted *MAPE* of K_{IC}^{S} is 4.56%, *RMSE* is 0.09 MPa·m$^{1/2}$, *a*15 is 100% and the covariance is 0.01 (MPa)^2 m. Furthermore, $MAPE = 11.46\%$, $RMSE = 0.11$ MPa $\cdot$ m$^{1/2}$, $a15 = 81.82\%$ and $Cov = 0.01$ (MPa)^{2}m of K_{IC}^{Q} indicate that the prediction accuracy of initiation and unstable toughness can meet the requirements of engineering applications.

Figure 11 shows the calculation results of the critical tip-opening displacement ($CTOD_c$) and the cohesive force ($F_{\sigma w}$) in the fracture process zone of specimens with different sizes and an initial α_c of 0.4. It can be seen from Figure 11 that $CTOD_c$ increases rapidly when the specimen height is less than 10 m. When the specimen height reaches 10 m, $CTOD_c$ tends to be stable, and the stable $CTOD_c$ is 47.4 μm. Similarly, $F_{\sigma w}$ first increases rapidly with the increase in specimen size and then tends to be stable at 42.4 kN.

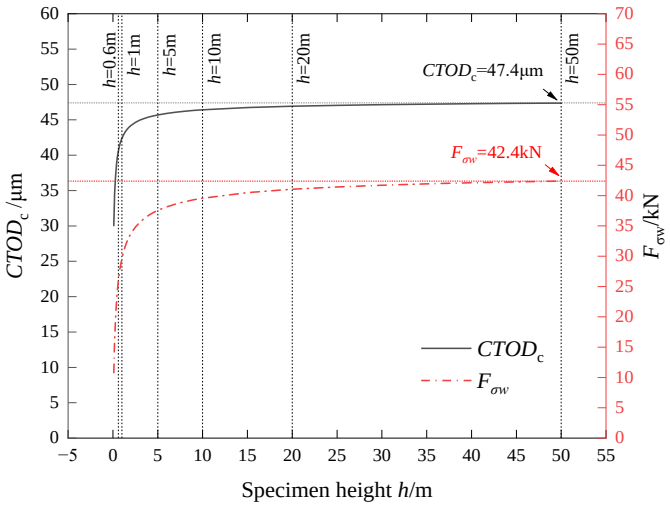

Figure 11. $CTOD_c$ and $F_{\sigma w}$ of specimens with different sizes.

Figure 12 shows the midspan section stress distribution of wedge-splitting tensile specimens with heights of 0.6, 1, 5, 20, 10, 20 and 50 m. In the figure, F_t is the tensile force of the uncracked zone in the midspan section of the specimen (kN), and F_c is the pressure-resultant force on the uncracked area of the midspan section of the specimen (kN).

It can be seen from the figure that with the increase in specimen size, F_t and F_c gradually increase. F_{sw} increases with the increase in size, and its growth rate gradually slows down and tends toward stability increased size.

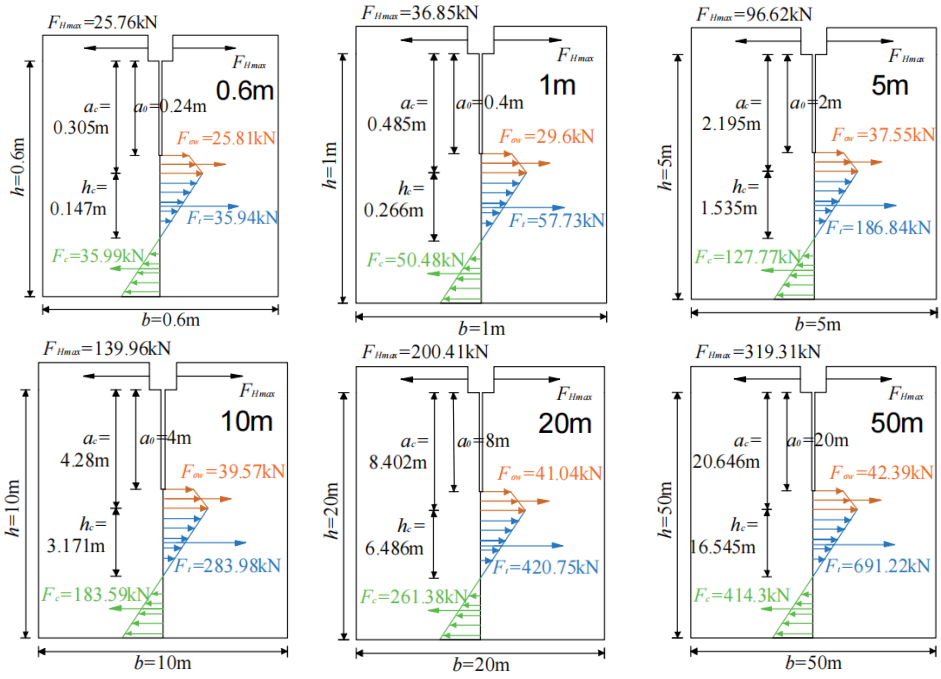

Figure 12. Stress distribution in the midspan section of specimens with different heights.

(2) α_0 = 0.4, h = 0.3~0.6 m

In reference [56], the fracture properties of wedge-splitting tensile specimens with an α_c of 0.4 and effective heights of 0.3, 0.4, 0.5 and 0.6 m were tested. Table 2 shows the specimen size and test results. Reference [56] reported the test results used to calculate the elastic modulus. The elastic modulus (E_c) required by the method proposed in this chapter was taken as the average value of the calculated elastic modulus, i.e., E_c = 39.05 GPa. Detailed test information is provided in reference [56].

Table 2. Fracture test results reported in reference [56].

Specimen Number	h/m	b/m	t/m	α_0	F_{Hmax}/kN	F_{HQ}/kN
WS300	0.3	0.3	0.2	0.4	11.793	7.003
WS400	0.4	0.4	0.2	0.4	15.067	9.342
WS500	0.5	0.5	0.2	0.4	17.766	10.953
WS600	0.6	0.6	0.2	0.4	21.253	13.43

Based on Equations (6) and (7), linear regression analysis of the test results was carried out, and the linear regression equations of $1/\left(\sigma_{Ne}^{Q}\right)^2$, $1/\left(\sigma_{Ne}^{S}\right)^2$ and a_e were obtained, as shown in Figure 13. According to the slope and intercept, K_{IC}^{ini} without a size effect is 1.47 MPa·m$^{1/2}$, c_f^{ini} is 460.6 mm, K_{IC}^{un} is 1.72 MPa·m$^{1/2}$ and c_f^{un} is 193.1 mm.

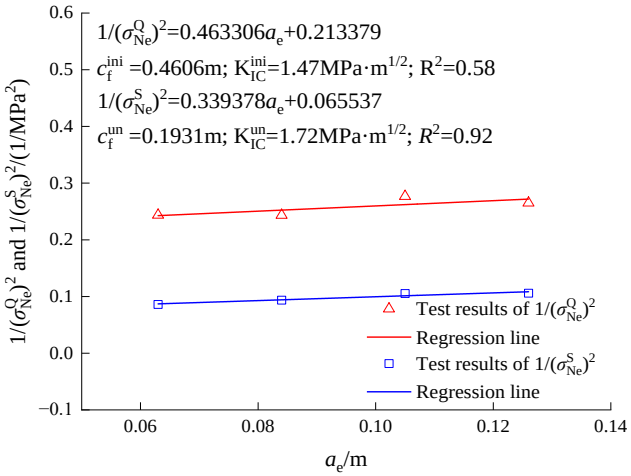

Figure 13. Linear relationships of $1/\left(\sigma_{Ne}^{Q}\right)^2$, $1/\left(\sigma_{Ne}^{S}\right)^2$ and a_e.

The K_{IC}^{ini} and c_f^{ini} and K_{IC}^{un} and c_f^{un} obtained by linear analysis are substituted into Equations (8) and (9), respectively, and the relationship between the initiation and peak loads with the equivalent geometric parameter (A_e) can be obtained as shown in Figure 14. In the figure, the slope of the initiation load prediction line is K_{IC}^{ini} without size effect, and the slope of the peak load prediction line is K_{IC}^{un} without a size effect. It can be seen from Figure 7 that the test results of F_{HQ} and F_{Hmax} are nearly linear relative to A_e. The *MAPE* of F_{HQ} prediction is 0.99%, *RMSE* is 0.22 kN, reliability index $a15$ is 100% and the covariance is 5.43 (kN)^2. The *MAPE* of F_{Hmax} prediction is 1.5%, *RMSE* is 0.19 kN, $a15$ is 100% and the covariance is 12.01 (kN)^2. The above indices show that the size effect model can realize the accurate prediction of initiation and peak loads when the size or α_c changes.

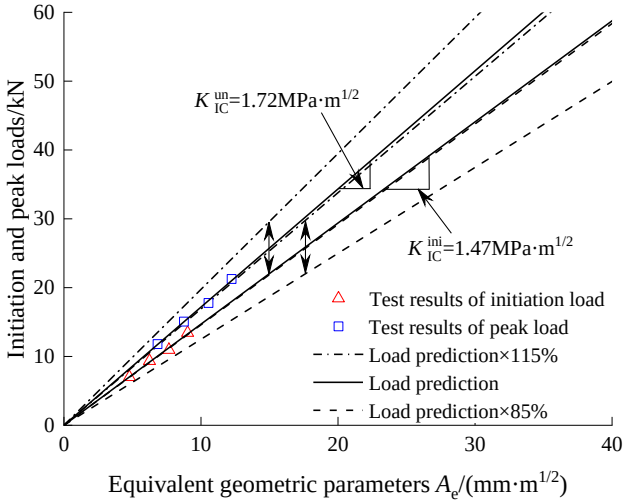

Figure 14. Predicted results of initiation and peak loads.

In order to evaluate the effectiveness of the proposed method, substituting the test results of initiation load into Equation (1), the calculated value is taken as the test value of initiation toughness. The test results of F_{Hmax} and a_c are substituted into Equation (3), and the calculated results are used as the unstable toughness test results. Then, these results are compared with the predicted results of initiation and unstable toughness calculated by the proposed method.

The optimal fitting softening parameter (w_0) was 450 mm, and $MAPE$ was 3.46%, as calculated by the proposed method. Figure 15 shows the predicted results of fracture parameters of specimens with an α_c of 0.4 and different sizes. It can be seen from Figure 15a that all data points of critical fracture length fall near the predicted line. It can be seen from Figure 15b that the data points of fracture toughness all fall near the corresponding fracture toughness prediction line; K_{IC}^{S}, K_{IC}^{N} and K_{IC}^{Q} all have a size effect. K_{IC}^{Q} is close to the initiation toughness without a size effect, i.e., 1.47 MPa·m$^{1/2}$. The predicted value of K_{IC}^{S} increases with an increase in size and then decreases slightly with a further increase in size. K_{IC}^{S} and K_{IC}^{N} approach one another with increased size, with values close to the unstable toughness without a size effect, i.e., 1.72 MPa·m$^{1/2}$. The accuracy evaluation indicators of a_c are $RMSE = 0.007$, $MAPE = 2.22\%$, $a15 = 100\%$ and $Cov = 0.003$ m^2; the accuracy evaluation indicators of K_{IC}^{Q} are $RMSE = 0.011$, $MAPE = 1.5\%$, $a15 = 100\%$ and $Cov = 0.004$ (MPa)^{2}m; the accuracy evaluation indicators of K_{IC}^{S} are $RMSE = 0.059$, $MAPE = 3.46\%$, $a15 = 100\%$ and $Cov = 0.004$ (MPa)^{2}m, which shows that the predicted results are more accurate. The proposed method can achieve accurate prediction of specific α_c, critical crack length, crack initiation toughness and unstable toughness of concrete specimens with different sizes and can also determine the initiation and unstable toughness without a size effect.

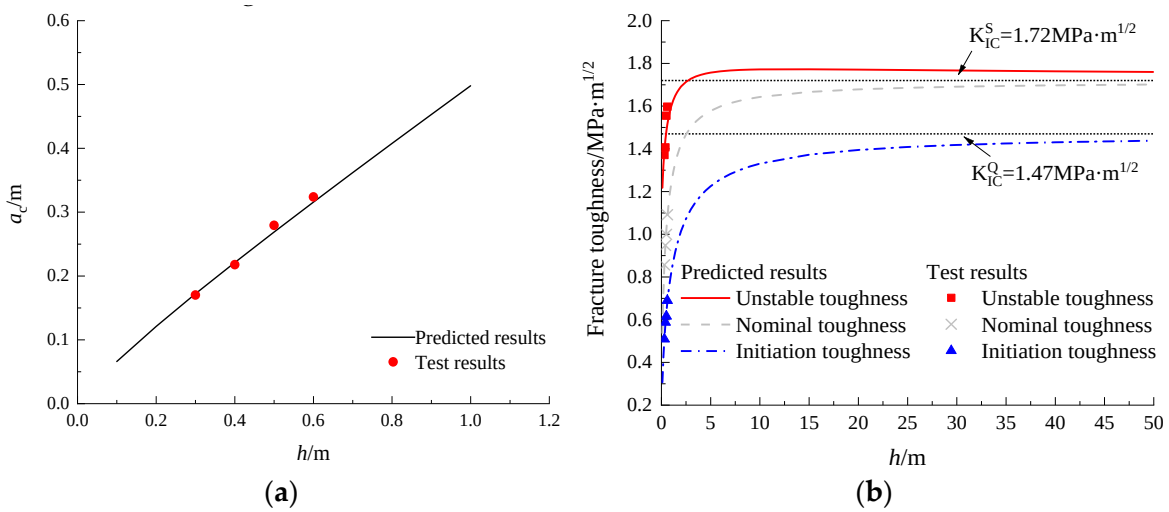

Figure 15. Critical crack length and fracture toughness of specimens with different sizes: (**a**) critical crack length; (**b**) fracture toughness.

3.1.2. Same Specimen Size but Different Crack Length-to-Height Ratio

In order to study the effect of initial α_c on the fracture performance of concrete, a wedge-splitting tensile fracture test was designed and carried out in reference [57] with maximum particle sizes of concrete aggregate of 10 mm and 20 mm, an effective specimen height of specimen of 0.3 m, a thickness of 0.12 m and an initial α_c in the range of 0.2 to 0.7. The specimen size and test results are summarized in Table 3. The compressive strength (f_{cu}) of a concrete cube with a maximum aggregate particle size of 10 mm is 42.2 MPa, and the elastic modulus is $E_c = 27.31$ GPa. The f_{cu} of a concrete cube with a maximum aggregate particle size of 20 mm is 57.04 MPa, with an elastic modulus of $E_c = 31.75$ GPa; the elastic modulus is calculated by f_{cu}. Additional experimental information can be found in reference [57].

Table 3. Fracture test results reported in reference [57].

Specimen Number	d_{max}/mm	*h*/*m*	*b*/*m*	*t*/*m*	α_0	F_{HQ}/kN	F_{Hmax}/kN
R0.2D10-1	10	0.3	0.3	0.12	0.2	10.03	13.32
R0.2D10-2		0.3	0.3	0.12	0.2	9.12	11.23
R0.2D10-3		0.3	0.3	0.12	0.2	11.05	14.27
R0.2D10-4		0.3	0.3	0.12	0.2	9.25	12.34
R0.4D10-1		0.3	0.3	0.12	0.4	6.94	8.72
R0.4D10-2		0.3	0.3	0.12	0.4	5.54	8.39
R0.4D10-3		0.3	0.3	0.12	0.4	5.46	8.38
R0.4D10-4		0.3	0.3	0.12	0.4	6.15	8.87
R0.6D10-1		0.3	0.3	0.12	0.6	2.90	4.30
R0.6D10-2		0.3	0.3	0.12	0.6	2.79	3.45
R0.6D10-3		0.3	0.3	0.12	0.6	3.57	4.43
R0.6D10-4		0.3	0.3	0.12	0.6	2.65	3.86
R0.7D10-1		0.3	0.3	0.12	0.7	1.93	2.54
R0.7D10-3		0.3	0.3	0.12	0.7	2.29	2.64
R0.7D10-4		0.3	0.3	0.12	0.7	2.02	2.74
R0.2D20-1	20	0.3	0.3	0.12	0.2	12.81	16.22
R0.2D20-2		0.3	0.3	0.12	0.2	10.66	15.48
R0.2D20-3		0.3	0.3	0.12	0.2	10.9	14.79
R0.2D20-4		0.3	0.3	0.12	0.2	12.71	16.83
R0.4D20-1		0.3	0.3	0.12	0.4	8.57	10.39
R0.4D20-2		0.3	0.3	0.12	0.4	7.21	9.84
R0.4D20-3		0.3	0.3	0.12	0.4	7.88	11.16
R0.4D20-4		0.3	0.3	0.12	0.4	8.06	11.10
R0.6D20-1		0.3	0.3	0.12	0.6	3.29	5.10
R0.6D20-2		0.3	0.3	0.12	0.6	3.56	4.58
R0.6D20-3		0.3	0.3	0.12	0.6	3.34	4.91
R0.6D20-4		0.3	0.3	0.12	0.6	3.47	4.80
R0.7D20-1		0.3	0.3	0.12	0.7	2.38	3.02
R0.7D20-3		0.3	0.3	0.12	0.7	2.56	3.13
R0.7D20-4		0.3	0.3	0.12	0.7	2.25	3.11

(1) d_{max} = 10 mm

Figure 16a,b show the linear relationship between $1/\left(\sigma_{Ne}^{Q}\right)^2$, $1/\left(\sigma_{Ne}^{S}\right)^2$ and a_e, as well as the predicted results of initiation and peak loads when the specimen size or α_c changes. According to the linear relationship shown in Figure 16a, K_{IC}^{ini} and K_{IC}^{un} without a size effect of concrete can be calculated as 0.93 MPa·m$^{1/2}$ and 1.22 MPa·m$^{1/2}$, respectively. Then, using Equations (8) and (9), the predicted lines of initiation and peak loads can be obtained. After calculation, the accuracy evaluation indicators of initiation load are $MAPE = 9.05\%$, $RMSE = 0.56$ kN, $a15 = 86.67\%$ and $Cov = 8.96$ (kN)^2; the accuracy evaluation indicators of peak load are $MAPE = 6.74\%$, $RMSE = 0.68$ kN, $a15 = 93.33\%$ and $Cov = 15.58$ (kN)^2. The calculation results show that the initiation and peak loads test results are close to the predicted results.

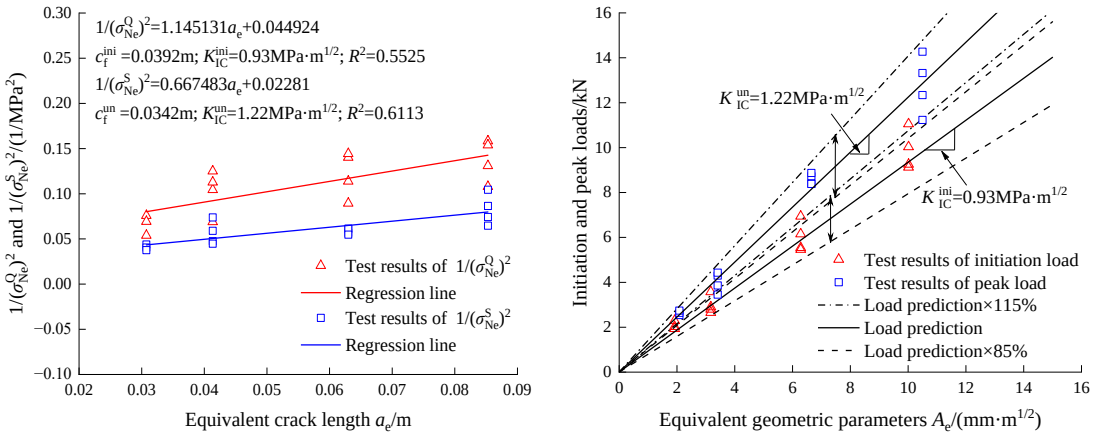

Figure 16. (**a**) Linear relationship of the size effect model; (**b**) predictions of initiation and peak loads.

After calculation, the w_0 obtained in this experiment is 150 μm, and the minimum value of *MAPE* of unstable toughness is 8.19%. Figure 17 shows the fracture toughness predicted results of specimens with different initial α_c value when the effective height of the specimen is 0.3 m. It can be seen from Figure 17 that the calculation results of K_{IC}^{Q} and K_{IC}^{S} basically decrease with an increase in the initial α_c, and most of the test results are within the allowable error range of ±15% of the predicted value. $MAPE = 8.19\%$, $RMSE = 0.16\ \text{MPa} \cdot \text{m}^{1/2}$, $a15 = 73.33\%$ and $Cov = 0.0003\ (\text{MPa})^2\text{m}$ of the corresponding K_{IC}^{S} predicted results. The above indices show that the determination method of fracture parameters based on the size effect model and fracture extreme theory can realize the accurate prediction of initiation and unstable toughness when the size or α_c changes.

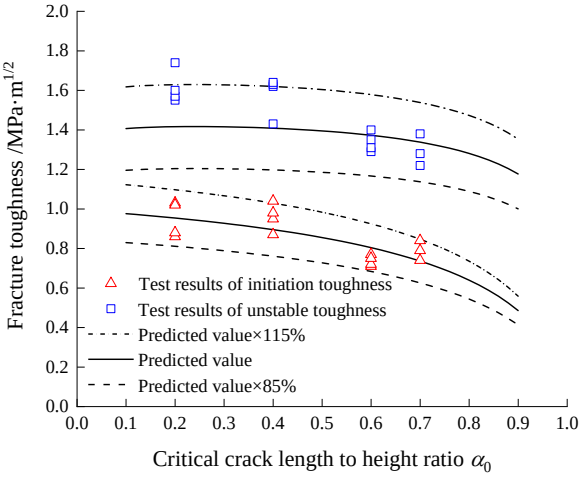

Figure 17. Fracture toughness of specimens with different α_0 values.

(2) d_{max} = 20 mm

Figure 18a shows the linear regression analysis of test results. According to the corresponding slope and intercept, K_{IC}^{ini} and K_{IC}^{un} without a size effect of concrete can be calculated as 1.21 MPa·m$^{1/2}$ and 1.63 MPa·m$^{1/2}$, respectively. Then, Equations (8) and (9) can be used to obtain the predicted line of initiation and peak loads with the slopes of K_{IC}^{ini} and K_{IC}^{un}, as shown in Figure 18b. After calculation, the accuracy evaluation indicators of initiation load are $MAPE = 7.95\%$, $RMSE = 0.66$ kN, $a15 = 93.33\%$ and $Cov = 13.66\ (\text{kN})^2$; the accuracy evaluation indicators of peak load are $MAPE = 4.51\%$, $RMSE = 0.60$ kN, $a15 = 100\%$

and $Cov = 24.75\ (\mathrm{kN})^2$. The calculation results show that the initiation and peak load test results are close to the predicted results.

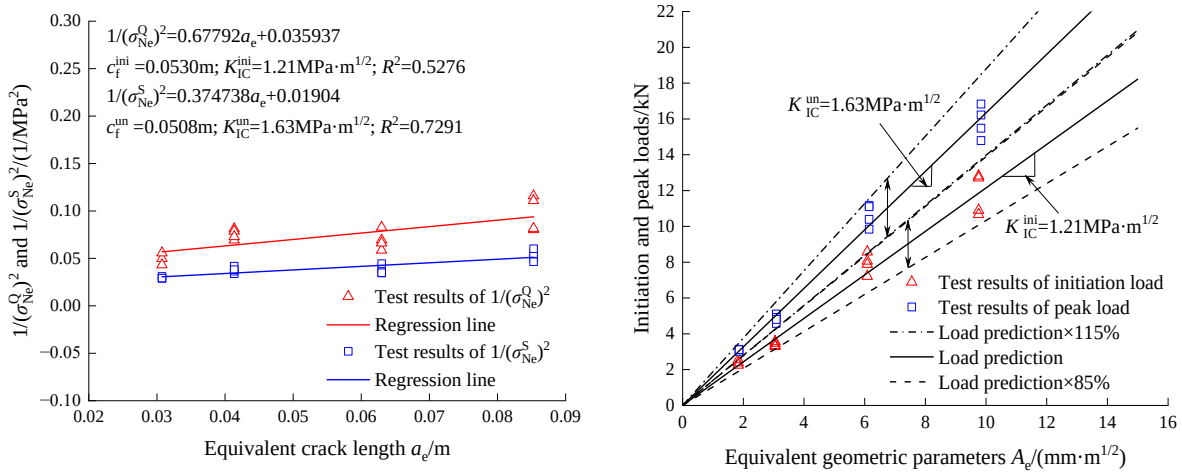

Figure 18. (**a**) Linear relationship of the size effect model; (**b**) predictions of initiation and peak loads.

After calculation, for the concrete with a maximum aggregate size of 20 mm, the optimal w_0 obtained by the test is 150 μm, and the minimum value of *MAPE* of unstable toughness is 7.91%. Figure 19 shows the fracture toughness predicted results of specimens with different initial α_c values when the effective height of the specimen is 0.3 m. It can be seen from Figure 19 that the calculated results of K_{IC}^{Q} and K_{IC}^{S} basically decrease with increased initial α_c, and most of the test results are within the allowable error range of ±15% of the predicted value. The corresponding K_{IC}^{Q} predicted results are $MAPE = 9.06\%$, $RMSE = 0.08\ \mathrm{MPa \cdot m^{1/2}}$, $a15 = 80.00\%$ and $Cov = 0.007\ (\mathrm{MPa})^2\mathrm{m}$. $MAPE = 7.91\%$, $RMSE = 0.12\ \mathrm{MPa \cdot m^{1/2}}$, $a15 = 93.33\%$ and $Cov = 0.004\ (\mathrm{MPa})^2\mathrm{m}$ of the predicted results of K_{IC}^{S}. The above indicators show that the fracture parameter determination method based on the size effect model and the fracture extreme theory can achieve more accurate prediction of initiation and unstable toughness when the size or α_c changes.

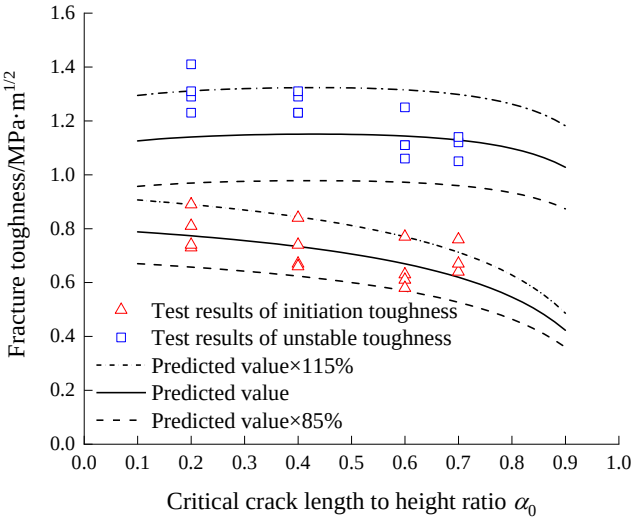

Figure 19. Fracture toughness of specimens with different α_0 values.

3.2. Fully Graded Concrete

Same Crack Length-to-Height Ratio and Different Specimen Sizes

In this section, the fracture test results of fully graded concrete of Wudongde Dam are analyzed to verify the applicability of the proposed method for fully graded concrete with a maximum aggregate size of 150 mm. The effective height of the Wudongde fully graded concrete wedge-splitting tensile specimens is 0.75 m, 1.5 m and 2.25 m; the initial α_c is 0.4; and the thickness is 0.45 m. The size and test results of concrete specimens are summarized in Table 4. Other experimental information can be found in reference [7].

Table 4. Test data reported in reference [2].

Specimen Number	*h*/m	*b*/m	*t*/m	α_0	F_{Hmax}/kN	F_{HQ}/kN
FG750-1	0.75	0.75	0.45	0.4	84.78	63.46
FG750-2	0.75	0.75	0.45	0.4	82.78	64.79
FG750-3	0.75	0.75	0.45	0.4	75.62	63.62
FG1500-1	1.5	1.5	0.45	0.4	157.44	117.46
FG1500-2	1.5	1.5	0.45	0.4	158.22	113.25
FG1500-3	1.5	1.5	0.45	0.4	158.43	110.11
FG2250-1	2.25	2.25	0.45	0.4	200.59	/
FG2250-2	2.25	2.25	0.45	0.4	200.67	140.04
FG2250-3	2.25	2.25	0.45	0.4	170.58	147.93

Figure 20a shows the linear relationship between $1/\left(\sigma_{Ne}^{Q}\right)^2$, $1/\left(\sigma_{Ne}^{S}\right)^2$ and a_e. Based on the slope and intercept of the linear equation, K_{IC}^{ini} and K_{IC}^{un} of the fully graded concrete without a size effect can be calculated as 2.12 MPa·m$^{1/2}$ and 2.90 MPa·m$^{1/2}$, respectively. Furthermore, combining Equations (8) and (9) and the obtained fracture toughness without a size effect, the initiation and peak load predicted lines shown in Figure 20b can be obtained. The indices selected in this paper can be used to evaluate the prediction accuracy of initiation and peak loads. After calculation, the evaluation indicators of initiation load are $MAPE = 2.51\%$, $RMSE = 3.62$ kN, $a15 = 100\%$ and $Cov = 1024.63$ (kN)^2; the evaluation indicators of peak load are $MAPE = 6.46\%$, $RMSE = 11.52$ kN, $a15 = 100\%$ and $Cov = 2032.55$ (kN)^2. The calculation results show that the predicted results of initiation and peak loads based on the size effect model are close to the test results.

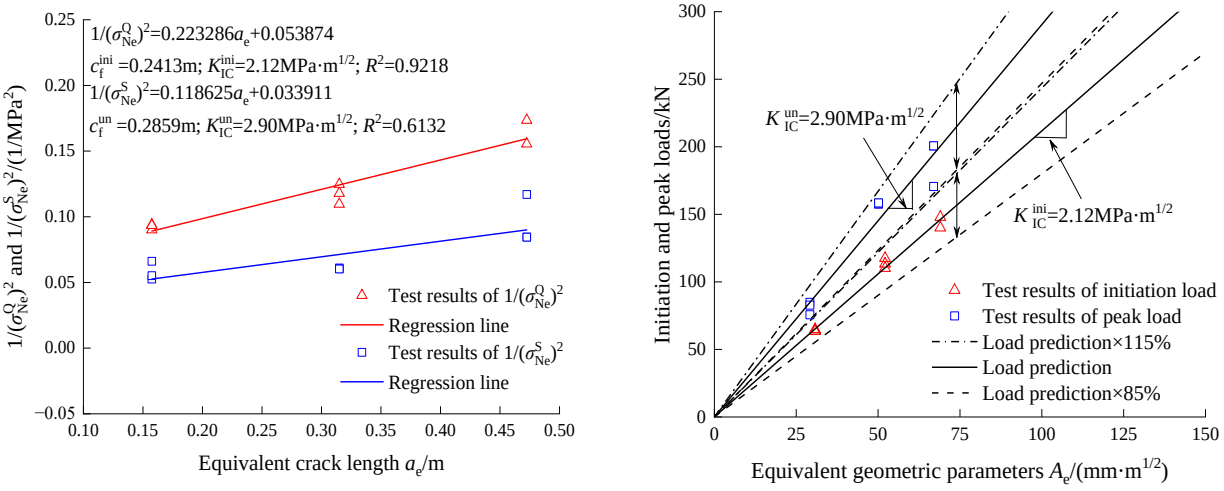

(**a**) (**b**)

Figure 20. (**a**) Linear relationship of the size effect model; (**b**) predictions of initiation and peak loads.

Figure 21a,b show comparisons between the predicted results and the test results of a_c, K_{IC}^{S}, K_{IC}^{N} and K_{IC}^{Q} of fully graded concrete specimens with different sizes and an initial α_c of 0.4 when the optimum w_0 is 350 μm. It can be seen from Figure 21a that the test results of a_c are close to the predicted results, and the prediction accuracy indices are $MAPE = 2.61\%$, $RMSE = 0.03$ m, $a15 = 100\%$ and $Cov = 0.06$ m^2. From Figure 21b, it can be seen that K_{IC}^{Q}, K_{IC}^{N} and K_{IC}^{S} increase with increased specimen size and tend toward K_{IC}^{ini} and K_{IC}^{un}, respectively without a size effect defined in the size effect model.

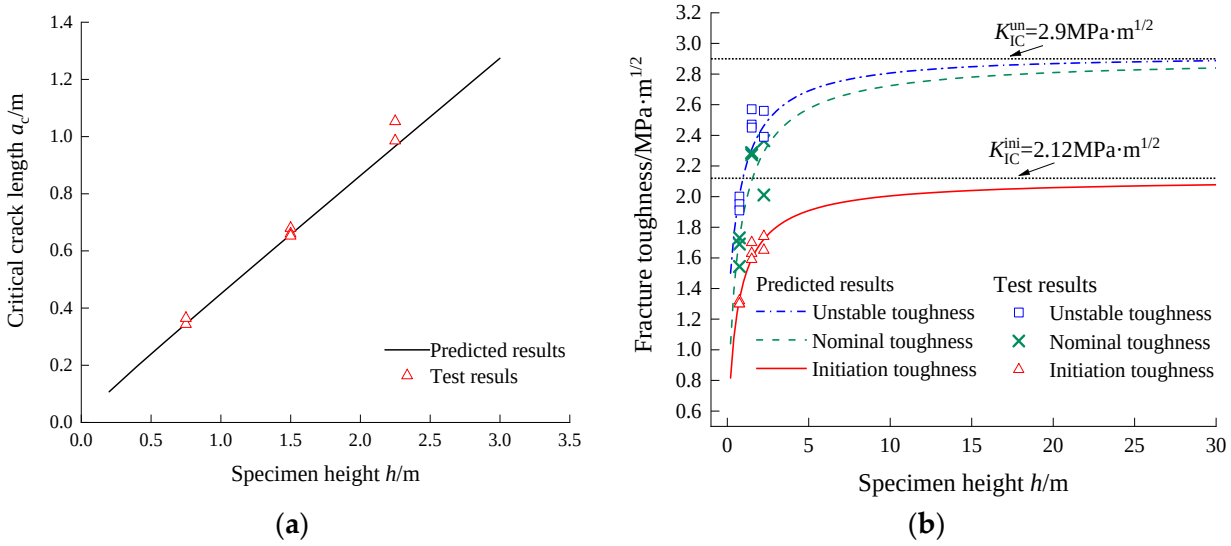

Figure 21. Critical crack length and fracture toughness of specimens with different sizes: (**a**) critical crack length; (**b**) fracture toughness.

Compared with the predicted results and test results of fracture toughness, the prediction accuracy evaluation indices of K_{IC}^{Q} are $MAPE = 2.44\%$, $RMSE = 0.05$ MPa $\cdot$ m$^{1/2}$, $a15 = 100\%$ and $Cov = 0.03$ (MPa)^{2}m. The above indicators show that the fracture parameter determination method proposed in this paper is also applicable to fully graded concrete, and the prediction accuracy can meet the needs of dam engineering.

Furthermore, based on the fracture test results of fully graded concrete with limited size, the proposed method can be used to determine the fracture toughness of specimens with a specific size and arbitrary initial α_c. Figure 22 shows a comparison between the predicted fracture toughness and the test results of specimens with different initial α_c values when the effective heights of specimens are 0.75 m, 1.5 m and 2.25 m. From Figure 22, it can be seen that K_{IC}^{Q} and K_{IC}^{S} decrease with increased initial α_c, and the test results are close to the predicted results. According to the evaluation index of prediction accuracy, the *MAPE* of fracture toughness is within 5%, and the maximum deviation of all predicted results is only 7.5%. It can be seen that the fracture parameter determination method proposed in this paper can accurately predict the fracture toughness of specimens with arbitrary size and α_c values only based on the limited size fracture test results.

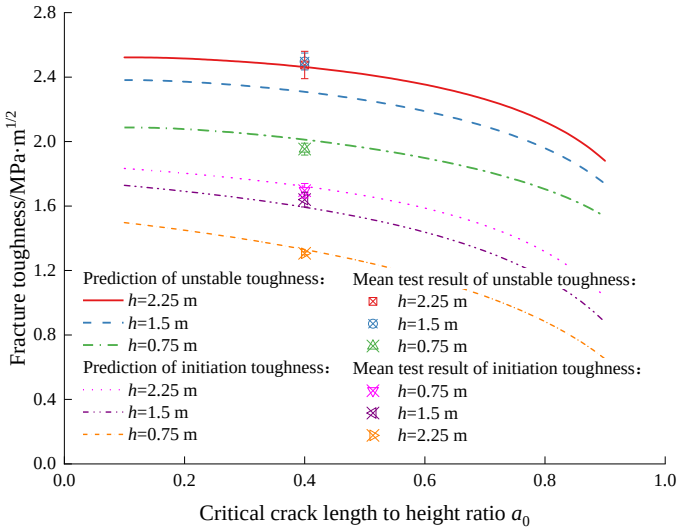

Figure 22. Fracture toughness of specimens with different α_0 values.

4. Conclusions

Combining the size effect model and the fracture extreme theory, in this paper, we propose a method to determine the double-*K* fracture toughness of concrete specimens with arbitrary size and α_c. The applicability and accuracy of the method were verified by the fracture test results of small aggregate concrete and Wudongde fully graded concrete. The main conclusions are as follows:

(1) Based on the wedge-splitting tensile test results of small aggregate concrete and fully graded concrete with limited size or α_c, the size effect model and fracture extreme theory can be used to accurately predict the initiation and peak loads, as well as the initiation and unstable toughness when the size or α_c changes. Furthermore, the prediction accuracy can meet the needs of engineering applications; the mean absolute percentage error is basically below 10%, most of the reliability indices are above 85% and the maximum can reach 100%. It can also be seen from the covariance that the predicted value is positively correlated with the test value.

(2) The K_{IC}^{Q}, K_{IC}^{N} and K_{IC}^{S} increased with increased specimen size and gradually stabilized. Furthermore, K_{IC}^{Q} tends toward K_{IC}^{ini} as defined in the size effect model. Both K_{IC}^{S} and K_{IC}^{N} tend toward K_{IC}^{un}, and the difference between the two gradually decreases with increased specimen size. The K_{IC}^{ini} and K_{IC}^{un} of the small aggregate concrete in example 1 in this paper are 1.14 MPa·m$^{1/2}$ and 1.81 MPa·m$^{1/2}$, respectively, and the K_{IC}^{ini} and K_{IC}^{un} of fully graded concrete are 2.12 MPa·m$^{1/2}$ and 2.9 MPa·m$^{1/2}$, respectively.

(3) The research results reported in this paper can provide a theoretical basis for the optimization of the fracture test. In dam engineering, we suggest carrying out fracture tests with limited size and α_c directly; the test results can then be analyzed using the method proposed in this paper. Then, the double-*K* fracture toughness of fully graded concrete specimens with arbitrary size can be determined. This method can be used for the analysis of the cracking risk and crack stability of dam structures in reality.

For dam concrete in actual service, its fracture parameters are not only affected by the size and crack length-to-height ratio of the specimen but also the age, maximum aggregate size, curing humidity and temperature, and other factors may also affect the fracture toughness of concrete. Therefore, in order to accurately evaluate the fracture parameters of dam concrete under actual service conditions, it is necessary to carry out research on the prediction of concrete fracture parameters considering additional factors in the future.

Author Contributions: Conceptualization, X.G.; Formal analysis, X.G., J.W. and T.X.; Funding acquisition, X.G.; Investigation, X.G. and J.W.; Methodology, X.G., M.Z., Y.T., N.Y., Y.Q., C.L., T.X. and J.W.; Supervision, X.G.; Validation, X.G.; Writing—original draft, X.G. and J.W.; Writing—review and editing, X.G., J.W. and T.X. All authors have read and agreed to the published version of the manuscript.

Funding: This research was funded by the National Natural Science Foundation of China (No. 52009123), the Zhejiang Provincial Natural Science Foundation of China (No. LY22E090004), the Open Research Fund Program of the State Key Laboratory of Hydroscience and Engineering (No. sklhse-2020-C-04) and Research Projects of China Three Gorges Corporation (Nos. BHT/0809, BHT/0806).

Data Availability Statement: The data presented in this study are available upon request from the corresponding author.

Conflicts of Interest: The authors declare no conflict of interest.

Nomenclature

K_{IC}^{Q}	Initiation toughness
K_{IC}^{S}	Unstable toughness
F_{HQ}	Initiation load
F_{Hmax}	Peak load
$f(\alpha_0)$	Dimensionless geometric parameter of the specimen
$Y(\alpha_0)$	Dimensionless geometric parameter of the specimen
a_c	Critical crack length
α_c	Crack length-to-height ratio ($\alpha_c = a_c/h$)
σ_N^Q	Nominal initiation strength
σ_N^S	Nominal unstable strength
σ_{Ne}^Q	Equivalent nominal initiation strength
σ_{Ne}^S	Equivalent nominal unstable strength
a_e	Equivalent crack length
K_{IC}^{ini}	Initiation toughness without size effect
c_f^{ini}	Effective length of the initiation fracture process zone
K_{IC}^{un}	Unstable toughness without size effect
c_f^{un}	Effective length of the unstable fracture process zone
F_{HQ}^{Pre}	Initiation load prediction
F_{Hmax}^{Pre}	Peak load prediction
$g'(\alpha_0)$	Dimensionless geometric parameter of the specimen
$g(\alpha_0)$	Dimensionless geometric parameter of the specimen
A_e^{ini}	Equivalent geometric parameter related to initiation
A_e^{un}	Equivalent geometric parameter related to instability
σ_c	Compressive stress at the bottom of the specimen
t	Thickness of specimen
h	Effective height of the specimen
a_0	Initial crack length
a	Effective crack length
h_c	Distance from the crack tip to the neutral axis marked by the dotted line
f_t	Equivalent tensile stress at the crack tip
σ_w	Cohesive force in the fracture process zone
CTOD	Crack-tip-opening displacement
CMOD	Crack-mouth-opening displacement
$w(x)$	Crack-opening displacement at x
w_s	Crack-opening displacement at the inflection point
w_0	Crack-opening displacement at zero cohesion
$\sigma_w(x)$	Cohesive force at x
σ_s	Cohesive force at a point
RMSE	Root mean square error
MAPE	Mean absolute percentage error

References

1. Li, Y.; Zhou, Y.; Wang, R.J.; Li, Y.L.; Wu, X.J.; Si, Z. Experimental investigation on the properties of the interface between RCC layers subjected to early-age frost damage. *Cem. Concr. Compos.* **2022**, *134*, 104745. [CrossRef]
2. Meng, T.; Lian, S.S.; Yu, H.M.; Yang, C.J.; Wang, M.H. Long-term influence of tailings wastewater on mechanical performance and microstructure of dam concrete: A case study in southeastern China. *Case Stud. Constr. Mater.* **2021**, *15*, e00720. [CrossRef]
3. Liu, W.J.; Tan, Y.S.; Li, Q.B.; Yang, N.; Liu, C.F.; Gao, X.F.; Hu, Y.; Niu, X.J.; Zhang, B. Influences of short-term heavy rainfall on interlayer properties and microstructure of concrete dam. *Case Stud. Constr. Mater.* **2022**, *14*, e01544. [CrossRef]
4. Qian, P.; Xu, Q.J. Experimental investigation on properties of interface between concrete layers. *Constr. Build. Mater.* **2018**, *174*, 120–129. [CrossRef]
5. Gao, X.F.; Hu, Y.; Yang, N.; Wu, K.; Li, Q.B. Fracture test and size effect analysis of low-heat cement fully-graded concrete. *Eng. Mech.* **2022**, *39*, 183–193. (In Chinese) [CrossRef]
6. Liu, W.J.; Wang, Y.B.; Li, Q.B.; Gao, X.F.; Tan, Y.S.; Liu, C.F.; Hu, Y.; Niu, X.J. Research on interlayer bonding quality control method of dam concrete based on equivalent age. *Materials* **2021**, *14*, 5192. [CrossRef]
7. Guan, J.F.; Li, Q.B.; Wu, Z.M.; Zhou, S.W. Necessity and Feasible Way of Studying True Fracture Parameters of Super-High Arch Dam Concrete. *J. Hydroelectr. Eng.* **2014**, *33*, 152–158. Available online: http://www.slfdxb.cn/CN/Y2014/V33/I5/152 (accessed on 15 July 2022). (In Chinese)
8. Kim, J.K.; Yun, L.; Yi, S.T. Fracture characteristics of concrete at early ages. *Cem. Concr. Res.* **2004**, *34*, 507–519. [CrossRef]
9. Xu, S.L.; Zhao, Y.H.; Wu, Z.M.; Gao, H.B. The experimental study on the fracture energy of concrete using wedge splitting specimens. *J. Hydroelectr. Eng.* **2003**, 15–22. (In Chinese) [CrossRef]
10. Hoover, C.G.; Bažant, Z.P. Comprehensive concrete fracture tests: Size effects of Types 1 & 2, crack length effect and postpeak. *Eng. Fract. Mech.* **2013**, *110*, 281–289. [CrossRef]
11. Beygi, M.H.A.; Kazemi, M.T.; Nikbin, I.M.; Amiri, J.V. The effect of water to cement ratio on fracture parameters and brittleness of self-compacting concrete. *Mater. Des.* **2013**, *50*, 267–276. [CrossRef]
12. Zhang, G.H.; Li, Z.L.; Nie, K.Y.; Liu, M.H. Experimental study on fracture toughness of concrete with different moisture contents. *J. Hydroelectr. Eng.* **2016**, 109–116. (In Chinese) [CrossRef]
13. Xu, S.L.; Li, Q.H.; Wu, Y.; Dong, L.X.; Lyu, Y.; Reinhardt, H.W.; Christopher, K.Y.L.; Ruiz, G.; Kumar, S.; Hu, S.W. Determination of double-K criterion for crack propagation in quasi-brittle fracture, Part II: Analytical evaluating and practical measuring methods for three-point bending notched beams. *Int. J. Fract.* **1999**, *98*, 151–177. [CrossRef]
14. Xu, S.L.; Reinhardt, H.W. Determination of double-*K* criterion for crack propagation in quasi-brittle fracture Part I: Experimental investigation of crack propagation. *Int. J. Fract.* **1999**, *98*, 111–149. [CrossRef]
15. Xu, S.L.; Reinhardt, H.W. Determination of double-*K* criterion for crack propagation in quasi-brittle fracture, Part III: Compact tension specimens and wedge splitting specimens. *Int. J. Fract.* **1999**, *98*, 179–193. [CrossRef]
16. *Norm for Fracture Test of Hydraulic Concrete*; China Electric Power Press: Beijing, China, 2005. (In Chinese)
17. Xu, S.L.; Li, Q.H.; Wu, Y.; Dong, L.X.; Lyu, Y.; Reinhardt, H.W.; Christopher, K.Y.L.; Ruiz, G.; Kumar, S.; Hu, S.W. RILEM Standard: Testing methods for determination of the double-K criterion for crack propagation in concrete using wedge-splitting tests and three-point bending beam tests, recommendation of RILEM TC265-TDK. *Mater. Struct.* **2021**, *54*, 1–11. [CrossRef]
18. Alam, S.Y.; Zhu, R.; Loukili, A. A new way to analyse the size effect in quasi-brittle materials by scaling the heterogeneity size. *Eng. Fract. Mech.* **2020**, *225*, 106864. [CrossRef]
19. Pirooznia, A.; Moradloo, A. Investigation of size effect and smeared crack models in ordinary and dam concrete fracture tests. *Eng. Fract. Mech.* **2020**, *226*, 106863. [CrossRef]
20. Yin, Y.Y.; Hu, S.W. Double-*K* fracture parameters of concrete in three point bending beams with small span-depth ratios. *Eng. Mech.* **2020**, *37*, 138–146 (In Chinese) [CrossRef]
21. Guan, J.F.; Li, Q.B.; Wu, Z.M.; Zhao, S.B.; Dong, W.; Zhou, S.W. Minimum specimen size for fracture parameters of site-casting dam concrete. *Constr. Build. Mater.* **2015**, *93*, 973–982. [CrossRef]
22. Guan, J.F.; Li, Q.B.; Wu, Z.M.; Dong, W. Determination of minimum size for double *K* fracture parameters of site-casting fully-graded hydraulic concrete. *J. Basic Sci. Eng.* **2016**, *24*, 1219–1231. (In Chinese) [CrossRef]
23. Guan, J.F. Fracture parameters of site-cast dam and sieved concrete. *Mag. Concr. Res.* **2016**, *68*, 43–54. [CrossRef]
24. Hu, X.Z.; Duan, K. Size effect and quasi-brittle fracture: The role of FPZ. *Int. J. Fract.* **2008**, *154*, 3–14. [CrossRef]
25. Hu, X.Z. An asymptotic approach to size effect on fracture toughness and fracture energy of composites. *Eng. Fract. Mech.* **2002**, *69*, 555–564. [CrossRef]
26. Hu, X.Z.; Wittmann, F. Size effect on toughness induced by crack close to free surface. *Eng. Fract. Mech.* **2000**, *65*, 209–221. [CrossRef]
27. Bažant, Z.P. Size effect in blunt fracture: Concrete, rock, metal. *J. Eng. Mech.* **1984**, *110*, 518–535. [CrossRef]
28. Bažant, Z.P. Scaling theory for quasibrittle structural failure. *Proc. Natl. Acad. Sci. USA* **2004**, *101*, 13400–13407. [CrossRef]
29. Hoover, C.G.; Bažant, Z.P. Comparison of the Hu-Duan boundary effect model with the size-shape effect law for quasi-brittle fracture based on new comprehensive fracture tests. *J. Eng. Mech.* **2014**, *140*, 480–486. [CrossRef]
30. Guan, J.F.; Yuan, P.; Hu, X.Z.; Qing, L.B.; Yao, X.H. Statistical analysis of concrete fracture using normal distribution pertinent to maximum aggregate size. *Theor. Appl. Fract. Mech.* **2019**, *101*, 236–253. [CrossRef]

31. Yao, X.H.; Li, L.L.; Guan, J.F.; Zhang, M.; Liu, Z.P.; Han, R.C.; He, S.H. Initial cracking strength and initial fracture toughness from three-point bending and wedge splitting concrete specimens. *Fatigue Fract. Eng. Mater. Struct.* **2021**, *44*, 601–621. [CrossRef]
32. Guan, J.F.; Liu, Z.P.; Yao, X.H.; Li, L.L.; He, S.H.; Zhang, M. Determination of the cracking strength tensile strength and double-K fracture parameters of concrete. *Eng. Mech.* **2020**, *37*, 124–137. (In Chinese) [CrossRef]
33. Guan, J.F.; Yin, Y.N.; Li, Y.; Yao, X.H.; Li, L.L. A design method for determining fracture toughness and tensile strength pertinent to concrete sieving curve. *Eng. Fract. Mech.* **2022**, *271*, 108596. [CrossRef]
34. Guan, J.F.; Li, C.M.; Wang, J.; Qing, L.B.; Song, Z.K.; Liu, Z.P. Determination of fracture parameter and prediction of structural fracture using various concrete specimen types. *Theor. Appl. Fract. Mech.* **2019**, *100*, 114–127. [CrossRef]
35. Wu, Z.M.; Yang, S.T.; Hu, X.Z.; Zheng, J.J. An analytical model to predict the effective fracture toughness of concrete for three-point bending notched beams. *Eng. Fract. Mech.* **2006**, *73*, 2166–2191. [CrossRef]
36. Wu, Z.M.; Yang, S.T.; Zheng, J.J. Analytical method for predicting effective fracture toughness of concrete and its size effect. *J. Hydraul. Eng.* **2006**, 795–800. (In Chinese) [CrossRef]
37. Qing, L.B.; Cheng, Y.H.; Guan, J.F. Simplified extreme method for determining initiation toughness of dam concrete. *J. Hydroelectr. Eng.* **2018**, *37*, 93–100. (In Chinese) [CrossRef]
38. Qing, L.B.; Cheng, Y.H.; Fan, X.Q.; Mu, R.; Ding, S.Q. An arc bending notched specimen for determining the mechanical and fracture parameters of concrete based on the FET. *Eng. Fract. Mech.* **2019**, *220*, 106639. [CrossRef]
39. Li, Y.; Qing, L.B.; Cheng, Y.H.; Ma, G.W. Determining the tensile strength of concrete for wedge splitting specimens based on the fracture extreme theory. *Theor. Appl. Fract. Mech.* **2020**, *108*, 102654. [CrossRef]
40. Qing, L.B.; Dong, M.W.; Guan, J.F. Determining initial fracture toughness of concrete for split-tension specimens based on the extreme theory. *Eng. Fract. Mech.* **2018**, *189*, 427–438. [CrossRef]
41. Qing, L.B.; Cheng, Y.H. The fracture extreme theory for determining the effective fracture toughness and tensile strength of concrete. *Theor. Appl. Fract. Mech.* **2018**, *96*, 461–467. [CrossRef]
42. Nie, Y.T.; Qing, L.B. The relationship between double-K parameters of concrete based on fracture extreme theory. *J. Theor. Appl. Mech.* **2020**, *58*, 59–71. [CrossRef]
43. Li, Y.; Qing, L.B.; Cheng, Y.H.; Dong, M.W.; Ma, G.W. A general framework for determining fracture parameters of concrete based on fracture extreme theory. *Theor. Appl. Fract. Mech.* **2019**, 102259. [CrossRef]
44. Qing, L.B.; Su, Y.M.; Dong, M.W.; Cheng, Y.H.; Li, Y. Size effect on double-K fracture parameters of concrete based on fracture extreme theory. *Arch. Appl. Mech.* **2020**, 427–442. Available online: https://link.springer.com/article/10.1007/s00419-020-01781-5 (accessed on 15 July 2022).
45. Qing, L.B.; Li, Q.B. A theoretical method for determining initiation toughness based on experimental peak load. *Eng. Fract. Mech.* **2013**, 295–305. [CrossRef]
46. Qing, L.B.; Tian, W.L.; Wang, J. Predicting unstable toughness of concrete based on initial toughness criterion. *J. Zhejiang Univ. -Sci. A* **2014**, *15*, 138–148. [CrossRef]
47. Qing, L.B.; Nie, Y.T.; Wang, J.; Hu, Y. A simplified extreme method for determining double-K fracture parameters of concrete using experimental peak load. *Fatigue Fract. Eng. Mater. Struct.* **2017**, *40*, 254–266. [CrossRef]
48. Gao, X.F.; Liu, C.F.; Tan, Y.S.; Yang, N.; Qiao, Y.; Hu, Y.; Li, Q.B.; Koval, G.; Chazallon, C. Determination of Fracture Properties of Concrete Using Size and Boundary Effect Models. *Appl. Sci.* **2019**, *9*, 1337. [CrossRef]
49. Qing, L.B.; Li, Q.B.; Guan, J.F.; Wang, J. Study of concrete fracture process zone based on fictitious crack model. *Eng. Mech.* **2012**, *29*, 112–116,132 (In Chinese) [CrossRef]
50. Wittmann, F.H.; Rokugo, K.; Brühwiler, E.; Mihashi, H.; Simonin, P. Fracture energy and strain softening of concrete as determined by means of compact tension specimens. *Mater. Struct.* **1988**, *21*, 21–32. [CrossRef]
51. Li, Q.B.; Deng, Z.C.; Fu, H. Effect of aggregate type on mechanical behavior of dam concrete. *ACI Mater. J.* **2004**, *101*, 483–492. Available online: https://www.concrete.org/publications/internationalconcreteabstractsportal/m/details/id/13487 (accessed on 15 July 2022).
52. *CEB-FIP Model Code 1990. Programs Usenix Unix Supplementary Documents. UK*; Redwood Books: Coconut Creek, FL, USA, 1993.
53. Reinhardt, H.W.; Cornelissen, H.; Hordijk, D.A. Tensile tests and failure analysis of concrete. *J. Struct. Eng.* **1986**, *112*, 2462–2477. [CrossRef]
54. Ding, X.T.; Ding, X.; Liu, H.X.; Zheng, Y. Comparison study on softening curve of concrete by direct tension test and three-point bending fracture test. *Water Resour. Power* **2014**, *32*, 116–118; 156. (In Chinese)
55. Zhang, X.F.; Xu, S.L. A comparative study on five approaches to evaluate double-*K* fracture toughness parameters of concrete and size effect analysis. *Eng. Fract. Mech.* **2011**, *78*, 2115–2138. [CrossRef]
56. Hu, S.W.; Xie, J.F. Experimental research and size effect analysis of fracture parameter of nonstandard wedge splitting tensile specimen. *Water Resour. Power* **2015**, *33*, 105–108. (In Chinese)
57. Du, M.; Wu, L.; Zhang, J.M. Effect of different initial crack-depth ratios and aggregate size on fracture properties of low-heated concrete. *Concrete* **2020**, 14–17. (In Chinese) [CrossRef]